Solution Structure of Bound Trimethoprim in Its Complex with Lactobacillus casei Dihydrofolate Reductase

9 AUTHORS, INCLUDING:

Gabriel Martorell
University of the Balearic Islands
22 PUBLICATIONS **637** CITATIONS

SEE PROFILE

H.T. A. Cheung
University of Sydney
95 PUBLICATIONS **1,263** CITATIONS

SEE PROFILE

Vladimir Polshakov
Lomonosov Moscow State University
70 PUBLICATIONS **521** CITATIONS

SEE PROFILE

James Feeney
MRC National Institute for Medical Research
315 PUBLICATIONS **7,804** CITATIONS

SEE PROFILE

Solution Structure of Bound Trimethoprim in Its Complex with *Lactobacillus casei* Dihydrofolate Reductase[†]

G. Martorell,[‡] M. J. Gradwell,[‡] B. Birdsall,[‡] C. J. Bauer,[§] T. A. Frenkiel,[§] H. T. A. Cheung,[⊥] V. I. Polshakov,[‡] L. Kuyper,[‖] and J. Feeney[*,‡]

Laboratory of Molecular Structure and MRC Biomedical NMR Centre, National Institute for Medical Research, The Ridgeway, Mill Hill, London NW7 1AA, U.K., Burroughs Wellcome Co., Research Triangle Park, North Carolina, and Department of Pharmacy, University of Sydney, New South Wales, Australia

ABSTRACT: Two- and three-dimensional (2D and 3D) NMR techniques have been used to assign the signals from nearly all of the protons in *Lactobacillus casei* dihydrofolate reductase (DHFR) (M_r 18 300) in its 1:1 complex with the antibacterial drug trimethoprim. A sample of uniformly ^{15}N-labeled protein was examined using 3D ^{15}N/^{1}H experiments [nuclear Overhauser, heteronuclear multiple quantum coherence (NOESY-HMQC) and total correlation, heteronuclear multiple quantum coherence (TOCSY-HMQC) experiments]. Twenty-two intermolecular NOEs between trimethoprim and protein protons and four intramolecular NOEs in the ligand have been detected. Some were obtained by using heteronuclear editing and 2D HMQC-NOESY experiments on complexes formed with [15]N- and ^{13}C-labeled trimethoprim molecules ([1,3-[15]N_2,2-*amino*-^{15}N]- and [7-^{13}C,4'-*methoxy*-^{13}C]trimethoprim) bound to unlabeled protein. The ligand–protein NOEs were used as distance constraints in conjunction with minimum energy and simulated annealing calculations (carried out with X-PLOR) to dock the trimethoprim ligand into dihydrofolate reductase, using as a starting structure the crystal coordinates from a related complex with a similar overall protein structure. The restrained minimum energy calculations and the simulated annealing calculations gave 83 calculated structures with distance violations of <0.1 Å. In all of these, the two aromatic rings of trimethoprim occupied essentially the same region of conformational space in the binding site (RMSD = 0.63 Å). The protein residues nearest to the bound trimethoprim were found to be very similar in all of the structures and agreed well with corresponding contact residues observed in the X-ray crystal studies on trimethoprim complexes formed with *Escherichia coli* and chicken liver DHFRs.

Dihydrofolate reductase (DHFR[1]) is an essential enzyme in all cells, where it catalyzes the reduction of dihydrofolate to tetrahydrofolate using NADPH as a coenzyme (Blakley, 1985). The enzyme is of considerable pharmacological interest, being the target for antifolate drugs such as trimethoprim (TMP) and methotrexate (MTX). There have been extensive studies aimed at trying to understand the specificity of ligand binding in complexes of dihydrofolate reductases formed with a variety of inhibitors. Binding studies have been reported for a wide range of inhibitors (Roth & Cheng, 1982), and a substantial amount of structural

information has been obtained mainly from X-ray crystallography and NMR studies [see the reviews of Blakley (1985), Freisheim and Matthews (1984), and Feeney (1990)]. For example, the X-ray-determined structures of the *Escherichia coli*, *Lactobacillus casei*, chicken liver, and human enzyme in binary and ternary complexes with ligands have been reported (Baker *et al.*, 1982; Bolin *et al.*, 1982; Filman *et al.*, 1982; Matthews *et al.*, 1985; Oefner *et al.*, 1988). Detailed NMR signal assignments have been made for complexes of the *L. casei* (Soteriou *et al.*, 1993; Carr *et al.*, 1991), *E. coli* (Falzone *et al.*, 1994), and human (Stockman *et al.*, 1992) enzymes, and information about the binding sites has been obtained from considerations of NOE and crystallographic structural data. Site-directed mutagenesis of the *E. coli* enzyme in combination with kinetic studies has also been used to characterize structure–function relationships (Mayer *et al.*, 1986; Villafranca *et al.*, 1983; Benkovic *et al.*, 1988).

One of the most studied ligands is the antibacterial drug, trimethoprim, which acts by selectively inhibiting dihydrofolate reductase in bacterial cells. The association constant for the formation of the binary complex of trimethoprim with DHFR from *L. casei* is 17 times greater than that for the same complex formed with the mammalian enzyme (Baccanari *et al.*, 1982). In the presence of NADPH, trimethoprim binds to the *L. casei* enzyme 200-fold more tightly than it does in the absence of NADPH. Baccanari and co-workers (1982) have shown that this cooperativity in ligand binding is much diminished in the case of the mammalian enzyme, where trimethoprim binds 3 orders of magnitude more weakly in the ternary complex. Clearly, the specificity of trimethoprim binding is controlled not only by the difference in binding in the

[*] Author to whom correspondence should be addressed.
[‡] Laboratory of Molecular Structure, National Institute for Medical Research.
[§] MRC Biomedical NMR Centre, National Institute for Medical Research.
[⊥] University of Sydney.
[‖] Burroughs Wellcome Co.

[1] Abbreviations: 2D, two-dimensional; 3D, three-dimensional; COSY, two-dimensional correlation spectroscopy; DANTE, delays alternating with nutation for tailored excitation; DHFR, dihydrofolate reductase; DQF-COSY, double-quantum-filtered correlation spectroscopy; enzyme, dihydrofolate reductase (EC 1.5.1.3); HMQC, heteronuclear multiple quantum coherence spectroscopy; HOHAHA, homonuclear Hartmann–Hahn spectroscopy; MTX, methotrexate; NADPH, reduced nicotinamide adenine dinucleotide phosphate; NOE, nuclear Overhauser effect; NOESY, two-dimensional nuclear Overhauser effect spectroscopy; RMSD, root mean square deviations; ROESY, rotating frame NOE spectroscopy; SCUBA, stimulated cross-peaks under bleached α's; TPPI, time-proportional phase incrementation; TOCSY, total correlation spectroscopy.

trimethoprim binary complex but also by the large difference in the cooperativity of binding in the presence of NADPH. However, explanations for these differences in binding and cooperativity at the detailed structural level are still unclear, despite previous structural and mutagenesis studies. Earlier comparisons of X-ray structures of the ternary complexes formed with the *E. coli* enzyme and with the chicken liver enzyme (Matthews *et al.*, 1985) had indicated structural differences between the bound trimethoprim in the two complexes. However, more recent X-ray studies on complexes with the mouse enzyme (Groom *et al.*, 1991) have not revealed substantial differences in the bound conformation of trimethoprim in the complexes formed with bacterial and mammalian enzymes. Previous NMR studies, based on interpreting the proton chemical shifts of bound trimethoprim in terms of ring current shielding contributions, both from protein aromatic residues and from the aromatic rings of trimethoprim itself, also indicated substantial differences in conformation between the trimethoprim in the binary complexes formed with bacterial (*L. casei*) and mammalian (L1210) dihydrofolate reductases (Birdsall *et al.*, 1983).

Further studies are required to understand the structural origins of the differences in binding, and a full understanding will be achieved only when structural information is available for the binary and ternary complexes. Advances in NMR technology and methodology over the last few years offer the possibility of obtaining detailed structural information in solution for proteins of the size of dihydrofolate reductase (18 000–20 000 molecular weight). Here we report on the sequence-specific assignments of resonances in complexes of trimethoprim with uniformly ^{15}N-labeled *L. casei* dihydrofolate reductase and on the use of isotopically labeled trimethoprim analogues to obtain NOE information between bound proton signals in trimethoprim and assigned proton signals from the protein. These experimentally obtained distance constraints allowed us to dock the trimethoprim molecule within its binding site in dihydrofolate reductase and to deduce information about the conformation of the bound trimethoprim and its contact residues in the protein.

MATERIALS AND METHODS

Materials. Unlabeled *L. casei* DHFR was prepared as described previously from an *E. coli* strain into which the structural gene for the *L. casei* enzyme had been cloned (Dann *et al.*, 1976; Andrews *et al.*, 1985). The ^{15}N-labeled protein was expressed in *E. coli* cells grown on minimal medium containing 10 g/L glucose, 1 g/L sodium citrate, 20 g/L potassium phosphate, 0.2 g/L magnesium sulfate, 40 mg/L L-tryptophan, 50 mg/L ampicillin, and 1 g/L 99% ^{15}N-enriched ammonium sulfate. L-Tryptophan was included in the growth medium since the *E. coli* strain used is auxotrophic for tryptophan; however, complete ^{15}N labeling of the amide nitrogen of the tryptophan residue occurred as a result of transaminase activity.

The 99% ^{15}N-enriched ammonium sulfate was obtained from Isotec Inc. (Miamisburg, OH), and 100 atom % D$_2$O and trimethoprim were obtained from Sigma. The syntheses of ^{13}C- and ^{15}N-labeled trimethoprim have been described previously (Smal *et al.*, 1986; Bevan *et al.*, 1985; Cresswell & Meutha, 1975). All other reagents used were of analytical reagent quality.

NMR Experiments. The NMR experiments were carried out on 0.5 and 0.6 mL samples of 1–5 mM DHFR–TMP in 500 mM potassium chloride and 50 mM potassium phosphate

buffer (pH* 6.5), made up with either D$_2$O or 90% H$_2$O/10% D$_2$O as appropriate (pH* values are pH meter readings uncorrected for deuterium isotope effects).

The experiments were performed on either a Varian UNITY 600 MHz or a Bruker AM 500 MHz spectrometer, with the probe temperature set to 308 K (except where indicated otherwise). All spectra were all acquired in the phase-sensitive mode using the methods of States *et al.* (1982) and TPPI (Marion & Wüthrich, 1983) for quadrature detection on the Varian and Bruker spectrometers, respectively. DQF-COSY (Rance *et al.*, 1983), TOCSY (Davis & Bax, 1985; Braun-schweiler & Ernst, 1983) with isotropic mixing times of 40–90 ms, and NOESY spectra (Jeener *et al.*, 1979; Macura *et al.*, 1981) with mixing times from 6 to 100 ms were recorded for both D$_2$O and H$_2$O samples of DHFR–TMP. The ^{15}N/^{1}H experiments carried out on uniformly ^{15}N-labeled DHFR were 2D HMQC (Mueller, 1979; Bax *et al.*, 1983), 3D TOCSY-HMQC (Marion *et al.*, 1989a) with an isotropic mixing time of 50 ms, 3D NOESY-HMQC (Marion *et al.*, 1989b), and 3D HMQC-NOESY-HMQC (Frenkiel *et al.*, 1990). The 3D NOESY-HMQC and HMQC-NOESY-HMQC spectra were both acquired with a 100 ms NOE build-up period. In the HMQC sections of the 2D and 3D experiments, the delays needed to allow evolution of ^{15}N–^{1}H coupling were set to 5 ms. The isotropic mixing in all of the TOCSY experiments was produced by using an MLEV17 sequence (Bax & Davis, 1985) with a field strength of approximately 7.1 kHz.

Water suppression in both the 2D and 3D experiments was achieved by the use of selective presaturation, with either continuous-wave irradiation or a DANTE sequence (Morris & Freeman, 1978). To prevent the recovery of the solvent signal during the mixing time of the NOESY-based experiments, a 180° proton pulse was applied at the center of this period. In order to observe signals involving α-CH protons resonating at or very close to the chemical shift of the water, many of the 2D and 3D experiments employed a 60 ms SCUBA sequence, immediately after the presaturation period, to allow the restoration of magnetization to the bleached α-CH protons by cross-relaxation from neighboring protons (Brown *et al.*, 1988).

The spectra from 2D NMR experiments were typically acquired over 1–2 days, collecting 512 t_1 increments, 64–192 scans per increment, and 2048 pairs of complex points per scan. For spectra recorded from D$_2$O samples of DHFR–TMP the spectral width was set to 12.8 ppm in both dimensions, while for H$_2$O samples a value of 14.0 ppm was used. The 3D ^{15}N/^{1}H spectra were recorded over 3.5–4 days, acquiring 136 × 64 increments for NOESY-HMQC, 128 × 44 increments for HOHAHA-HMQC, and 136 × 60 increments for HMQC-NOESY-HMQC, with 16 transients per increment and 512 points per transient. In the NOESY-HMQC and HOHAHA-HMQC experiments, the spectral widths in F_1, F_2, and F_3 were 13.9, 35.3, and 7.1 ppm, respectively. The spectral widths used for the HMQC-NOESY-HMQC experiments were 35.3 ppm in F_1 and F_2 and 7.1 ppm in F_3.

Processing of 2D data was carried out using standard Bruker and Varian NMR software. No baseline correction was required. The original data were usually zero-filled once in F_2 and twice in F_1, while mild resolution enhancement was achieved by applying shifted sine or sine-squared apodization functions in both dimensions.

The 3D data were transformed, displayed, and plotted using software written in-house. The data were extended by factors of between 1.5 and 2.0 by linear prediction (Press *et al.*, 1988)

and then zero-filled once in all dimensions and multiplied by a sine-squared window function shifted by $\pi/2.5$.

For the one-dimensional NOE difference spectroscopy experiments, the spectra were collected with 16 000 data points over a spectral width of 14 400 Hz. A total of 126 blocks, each containing 64 transients, was collected. The N1H signal of trimethoprim could be specifically irradiated because it does not overlap any other signal in the spectrum (chemical shift, 14.9 ppm). This experiment was carried out at 298 K to sharpen the N1H signal by reducing the proton exchange rate between the N1H and water. The 1331 binomial sequence was used to avoid exciting the water resonance. The experiment was performed with three different irradiation times (0.8, 0.4, and 0.2 s). The peak intensities were corrected to compensate for the effects of the binomial sequence (Wagner & Wüthrich, 1979).

2D NOESY experiments with ^{15}N editing in ω_2 were carried out on DHFR complexes formed with [1,3-^{15}N$_2$,2-amino-^{15}N]trimethoprim. The spectra were acquired at 600 MHz using the following sequence: $90°(^1H)–t_1/2–180°(^{15}N)–t_1/2–90°(^1H)–\tau_m/2–180°(^1H)–\tau_m/2–90°(^1H)–\tau–180°(^1H), 90°(^{15}N),90°(^1H)–\tau–t_2$(acquire) (Wider et al., 1990). Heteronuclear broad-band decoupling was applied during the detection period by means of a GARP sequence (Shaka et al., 1985). A total of 800 t_1 increments with 96 scans per increment was acquired, using values for τ_m of 40–100 ms. Suppression of the residual solvent signal was achieved as described earlier.

The $^1H/^{13}C$ 2D HMQC-NOESY experiments were carried out on a Bruker AM 500 MHz spectrometer at 303 K using the sequence proposed by Gronenborn et al. (1989a,b), but without decoupling ^{13}C during the acquisition. The mixing time used was 100 ms. A total of 256 increments each with 96 scans was collected.

Molecular Modeling. Heavy atom coordinates of DHFR were extracted from the X-ray crystallographic data obtained for the *L. casei* DHFR–methotrexate–NADPH complex by Bolin et al. (1982). Hydrogen atoms were added within X-PLOR using the Hbuild subroutine (Brunger et al., 1988). A structure of the ligand, trimethoprim (**1**), was created using the builder module of the Insight II program within the Biosym package (Biosym Ltd.).
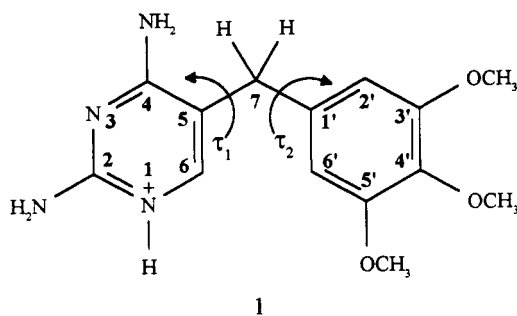
1

Two approaches were used for the modeling: one based on a restrained energy minimization procedure and the other based on a simulated annealing/energy minimization approach. The restrained energy minimization procedure was similar to the method of Weber et al. (1992) and was carried out in two stages. The first stage removes any bad atom-atom van der Waals contacts and consists of minimization of the following energy terms in X-PLOR for 100 cycles:

$$E_{total} = E_{bond} + E_{angle} + E_{impr} + E_{dihe} + E_{cdih} + E_{nonb}$$

The first four contributions are the bond, geometric angle, improper angle, and dihedral angle terms derived from the

X-PLOR energy function on the basis of the CHARMM force field. The term E_{nonb} is a quadratic repulsion potential that was used to account for nonbonded interactions. A force constant of 4 kcal mol^{-1} Å^{-2} was used, and the van der Waals radii were set at 0.9 of their values. In calculations on the trimethoprim complex, the additional term E_{cdih} is a quadratic potential used to fix the dihedral angles C2'–C3'–O3' (CH$_3$) and C4'–C5'–O5' (CH$_3$) in trimethoprim (**1**) at 273 K. An arbitrary value of 90 kcal mol^{-1} deg^{-2} was found to be effective for this term. Lennard-Jones potentials calculated for the structures after this stage were negative, indicating that any bad contacts had been removed.

The second stage involves minimization of the first five of these terms as well as E_{L-J}, the Lennard-Jones potential. A term for the experimental restraints, E_{NOE}, was also included using appropriate distance constraints in the form of a square-well potential. The force constant K_{NOE} was increased from 50 to 90 kcal mol^{-1} Å^{-2} in steps of 10 kcal mol^{-1} Å^{-2}, with 400 cycles for each value. This total of 2000 cycles was found to be the optimum value. Larger numbers yielded no considerable change in the total energy. From the initial ensemble only those optimized structures that possessed good geometries and satisfied all of the experimental restraints (to within 0.1 Å) were considered. The energy minimizations were carried out using X-PLOR 2.1 and 3.1 (Brünger, 1988, 1992) on a Sun SPARC station 10 Model 41.

In the second approach, a simulated annealing method was used that was based on a protocol for refinement of protein structures described by Nilges (1992). Prior to the dynamics, 100 steps of unrestrained energy minimization were performed on each structure. Complexes were then subjected to a total of 5 ps of simulated annealing in time steps of 1 fs, where initially only the drug molecule was allowed to move. The temperature was reduced from 1000 to 100 K in steps of 50 K. The NOE and constrained dihedral angle force constants were kept at values of 50 kcal mol^{-2} Å^{-2} and 200 kcal mol^{-2} rad^{-2}, respectively. A hard-sphere potential was used to represent nonbonded interactions. The force constant for this term was initially set at a small value (0.003 kcal mol Å^{-4}) and was progressively scaled during the dynamics to a final value of 4 kcal mol Å^{-4}. In an analogous manner, the hard-sphere radii were scaled from 0.9 to 0.75 times their van der Waals values. During the simulated annealing, the bond lengths were constrained using the SHAKE method (Rykaert et al., 1977; van Gunsteren & Berendsen, 1977). Finally, all atoms in the complex were allowed to relax for 1000 cycles of Powell minimization.

The structures of the enzyme–ligand complexes were displayed and manipulated using the Insight II program within the Biosym package (Biosym Ltd.) on a Silicon Graphics INDIGO R4000 Elan/XZ.

RESULTS AND DISCUSSION

In any NMR structural study of a protein–ligand complex, the first step is to assign the resonances of both the protein and the ligand. In the present work, we have applied multidimensional NMR experiments, including 3D TOCSY-HMQC and NOESY-HMQC experiments, to the complex of uniformly ^{15}N-labeled DHFR with trimethoprim in order to obtain the sequential resonance assignments and information about the structure in solution.

Protein Signal Assignments. The protein signal assignments for the DHFR–trimethoprim complex were made using established procedures (Wüthrich, 1986). Groups of resonances corresponding to single amino acid systems were first identified in the spectra and then assigned to particular residue

types in the protein. This was achieved by observing the scalar through-bond connectivities detected in 2D and 3D COSY and HOHAHA-based experiments. Sequence-specific assignments were then obtained by correlating sequence and NMR information in the manner used by Wüthrich and co-workers (Wüthrich, 1986). In this approach, protons in neighboring residues in the protein sequence are identified by detection of the NOEs between protons in residues i and i + 1 in 2D and 3D NOESY and ROESY type experiments. The secondary structure elements (four α-helices and an eight-stranded β-sheet) are also determined from these measurements. In earlier studies, we made detailed ^{1}H assignments for the binary complex of DHFR with methotrexate on the basis of experiments using uniformly ^{15}N- and ^{13}C-labeled enzymes (Soteriou *et al.*, 1993; Carr *et al.*, 1991) and noted secondary structural elements identical to those in the DHFR–trimethoprim complex. The earlier assignments for DHFR–methotrexate proved useful, assisting in the detailed assignments of some of the long chain amino acids in the DHFR–trimethoprim complex. By using these various approaches, an essentially complete list of sequence-specific resonance assignments was obtained for the protein signals in the DHFR–trimethoprim complex, and these assignments are given in Table 1. It is worth noting that the nonexchangeable NH protons assigned in the complex are the same as those in the DHFR–methotrexate complex, indicating similar patterns of hydrogen bond formation in the two complexes.

Ligand Signal Assignments. Some of the assignments for signals from bound trimethoprim have been made previously by using transfer of saturation experiments to connect corresponding signals in the bound and free ligand; the assignment for the H6, H2′,6′ and 3′,5′-OCH$_3$ protons were obtained in this way (Cayley *et al.*, 1979). The availability of the selectively ^{15}N- and ^{13}C-labeled trimethoprim molecules (**2** and **3**) also allows unequivocal assignments to be made for

2

3
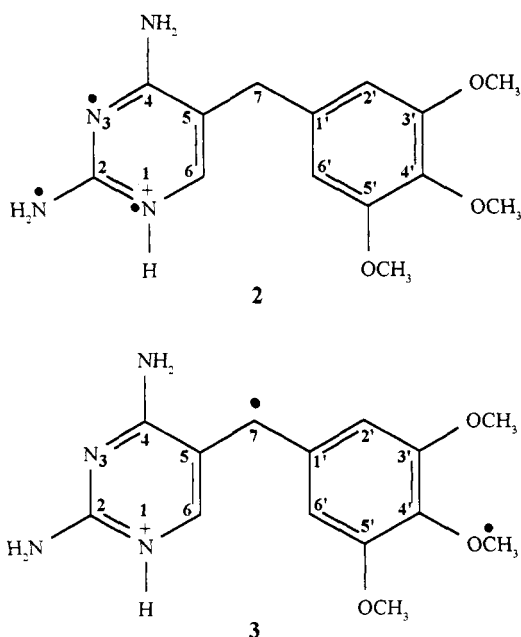
signals from the bound ligand. Heteronuclear editing and multiple quantum coherence experiments can be used to correlate and assign protons bonded to ^{15}N and ^{13}C; the N1H, 2-NH$_2$ (A and B), H7 (A and B), and 4′-OCH$_3$ proton signals were assigned in this way. The 4-NH$_2$ (A and B) proton signals could be detected in the 2D NOESY spectra from their characteristically shaped cross-peaks and NOE con-

nections to the assigned H7 (A and B) signals. The ^{1}H signal assignments for bound trimethoprim are given in Table 2.

Similarity of the Protein Structures in the Trimethoprim–DHFR and Methotrexate–DHFR Complexes. The availability of essentially complete lists of proton signal assignments for these two complexes allows us to make a detailed comparison of their chemical shifts and NOE connections. A total of 773 signals has been compared, and only 71 signals have chemical shift differences between the two complexes that are greater than 0.1 ppm: these are indicated in Table 1. An overall picture of where the chemical shift differences are found in the protein is obtained by computing the average of the sum of the RMS of the shift differences for each residue and plotting this as a function of residue number. Such a plot is shown in Figure 1. It is seen that the shifts in most of the residues are unchanged between the two complexes and that the chemical shift differences (RMS > 0.05 ppm) are largely confined to a few well-defined regions of the protein: the differences are concentrated around residues 21–37 and 45–57. Furthermore, an examination of the NOE cross-peaks in the 3D NOESY-HMQC spectra between all the signals indicates that very similar NOEs are seen for the vast majority of signals in the two complexes (98% of the 1500 NOEs examined are the same within the classification of strong, medium and weak). Figure 2a,b shows two corresponding slices taken from the 3D ^{15}N/^{1}H NOESY-HMQC spectra of the two complexes, DHFR-trimethoprim and DHFR-methotrexate. The patterns of NOEs are seen to be very similar for most NH protons. It is apparent that the overall structure of the protein in the two complexes remains relatively unchanged when methotrexate is replaced by trimethoprim.

Because of some structural similarities of the two drug molecules, it is reasonable to assume that parts of each molecule will occupy approximately the same binding region in the protein. However, each drug will have some different interactions with the protein: for example, methotrexate has a glutamic acid moiety that interacts with the protein in a way not available to trimethoprim. Thus, the shift differences observed around His 28 and Arg 57 (see Figure 1) are not unexpected in view of their involvement in the methotrexate glutamic acid interactions. [The crystal structure studies of Bolin *et al.* (1982) indicated that the MTX γ- and α-carboxylates interact with His 28 and Arg 57, respectively]. Furthermore, each drug will exert different ring current shielding effects on neighboring protons in the protein. Methotrexate has three aromatic rings, whereas trimethoprim has two: only one of the aromatic rings in each can occupy exactly the same binding site in the two complexes. One therefore can reasonably expect that the protein protons in close proximity to the bound drug molecules will show changes in chemical shifts between the two complexes, and these are indicated by asterisks in Figure 1.

Thus, the observed ^{1}H shift differences are mainly concentrated in the vicinity of the binding site and do not imply that the overall conformation of the protein is different in the two complexes. In fact, the observed similarities in the protein NOE data, the secondary structure elements, and the nonexchangeable NH protons all indicate that the overall conformation of the protein is similar in the two complexes. The NMR data for the binary methotrexate complex of DHFR show that the structure is similar to the X-ray structure of the methotrexate–NADPH–DHFR complex (Birdsall *et al.*, 1990; Carr *et al.*, 1991; Soteriou *et al.*, 1993). Thus, it is reasonable to use the X-ray structure (Bolin *et al.*, 1982) as a starting point for the docking experiments with trimethoprim.

Table 1: ¹H and ¹⁵N Resonance Assignments for the *L. casei* DHFR–TMP Complex[a]

residue	¹⁵N	HN	Hα	Hβ	Hβ'	Hγ	Hγ'	Hδ	Hδ'	other
1 Thr			4.18	4.44			1.23			
2 Ala	132.7	8.79	5.94	1.53						
3 Phe	120.6	8.89	5.94	3.53	3.25			6.77		7.06 (ε), 7.47 (ζ)
4 Leu	125.6	8.84	6.21	1.41[b]	2.06	2.37		1.19	0.65[b]	
5 Trp	127.5	9.28	5.50	3.60	3.52					11.09 (ε1), 6.97 (δ1), 7.17 (ε3), 6.71 (ζ3), 6.60 (η2), 7.37 (ζ2)
6 Ala	122.0	8.62	5.38	1.42						
7 Gln	114.6	9.03	6.28	1.93	2.37					
8 Asp	120.0	8.40	4.65	4.20	2.86					
9 Arg	115.4	7.69	4.14	1.83	1.60					
10 Asp	118.9	8.40	5.01	2.71	2.99					
11 Gly	107.2	7.95	3.51, 4.60							
12 Leu	125.3	9.08	4.36	1.92	1.72	1.69		0.94	0.82	
13 Ile	112.1	8.97	5.30	2.33		1.14	0.68	0.90		1.30 (γ2)
14 Gly	106.1	7.49	3.76, 4.35							
15 Lys	122.6	8.62	4.34	1.72	1.43	1.28	1.13			
16 Asp	130.9	10.34[b]	4.26	2.95	2.44					
17 Gly	104.7	9.10[b]	3.93, 3.38							
18 His	117.1	7.83	4.98	3.26	3.26					8.51 (ε1), 7.30 (δ2)
19 Leu						1.33		0.69	0.40	
20 Pro										
21 Trp	111.1	5.64	4.63							10.16 (ε1)[b], 6.44 (δ1), 6.14 (ε3)[b], 6.62 (ζ3), 7.44 (η2)[b], 7.03 (ζ2)
22 His	120.0	8.69	5.01	2.85	3.21					8.07 (ε1), 7.17 (δ2)
23 Leu	125.9	8.73[b]	4.83	2.04[b]	1.04	1.04		0.68	0.04	
24 Pro				2.30	1.90					
25 Asp	114.3	8.77[b]	4.47[b]	3.07	2.30					
26 Asp	117.2	6.98	5.31	2.29	2.65[b]					
27 Leu	119.5	7.47	4.21[b]	2.05[b]	0.95[b]	1.73[b]		0.95[b]	0.62[b]	
28 His	120.8	8.24[b]	4.55	3.37[b]	3.37[b]					7.87 (ε1)[b], 7.06 (δ2)[b]
29 Tyr	124.1	8.19[b]	4.19	3.13	3.38			6.78		6.66 (ε)
30 Phe	120.0	9.38[b]	3.69	3.02[b]	3.43			6.78		7.09 (ε), 7.32 (ζ)
31 Arg	120.5	7.83[b]	3.45[b]	2.20	2.17					
32 Ala	121.6	7.85	3.98	1.35						
33 Gln	112.2	7.93	4.05	1.36	1.36	1.97[b]	1.97[b]			
34 Thr	104.3	7.16[b]	4.16	3.62			0.36			
35 Val	121.2	7.59[b]	3.69[b]	1.98		1.01	0.96			
36 Gly	112.1	9.23	3.90, 4.19							
37 Lys	119.8	7.74[b]	4.73							
38 Ile	119.1	8.39	4.15	1.85						
39 Met	129.5	8.77	5.17	2.17	2.43					2.14 (ε)
40 Val	128.8	9.05	5.05	1.78		0.68	0.60			
41 Val	120.4	9.11	5.48	2.24		1.12[b]	0.91			
42 Gly	106.3	8.21	4.11, 4.61							
43 Arg	119.0	8.57	3.54	1.25	1.50	1.05				
44 Arg	117.0	8.19	3.86	1.89	1.82	1.68	1.58	3.14	3.14	
45 Thr	119.0	7.76	3.47[b]	3.91[b]			0.67[b]			
46 Tyr	121.0	8.03[b]	3.20[b]	2.83				6.94		
47 Glu	111.7	8.05	3.57	1.86	2.08	2.80	2.30			
48 Ser	114.8	7.33[b]	4.27	3.79[b]	3.93					
49 Phe	121.9	7.08	4.89	2.92	2.90			6.83		6.47 (ε), 6.87 (ζ)[b]
50 Pro										
51 Lys	115.7	7.18[b]	4.34	1.67	1.60	1.33				2.97 (ε)
52 Arg	119.4	8.11	4.38	1.34	1.30	1.04	1.04			
53 Pro										
54 Leu	121.9	9.44[b]	4.48[b]	1.42[b]	1.07	1.49[b]		0.25[b]	0.63[b]	
55 Pro			4.53	2.06	2.39					
56 Glu	114.0	9.14	3.91	2.20	2.35	2.14	2.06			
57 Arg	111.9	7.71	4.65							5.98 (ε)[b]
58 Thr	118.9	8.46	4.39	4.12			1.11			
59 Asn	127.5	9.65	4.99	3.10	2.23					
60 Val	126.0	9.17	4.81	1.84		0.58	0.34			
61 Val	126.9	8.68	4.65	1.53		0.44	−0.17			
62 Leu	128.7	8.10	4.75	0.71	1.50	1.14		0.42	0.65	
63 Thr	119.8	8.44	4.73	3.71			0.90			
64 His			4.77							8.33 (ε1), 7.30 (δ2)
65 Gln	122.2	8.33	4.13	2.07	2.03	2.33	2.33			
66 Glu	127.5	8.70	3.31	1.89	1.84	2.19	1.98			
67 Asp	116.1	8.39	4.63	2.91[b]	2.81					
68 Tyr	121.2	7.16	4.16	2.91	2.59			6.87		6.62 (ε)
69 Gln	126.2	7.56	4.31	1.72	1.87	2.26	2.26			
70 Ala	126.4	8.25	4.35	1.07						
71 Gln	123.7	8.53	4.12	2.03	2.03	2.38	2.38			
72 Gly	113.2	8.92	3.72, 4.12[b]							
73 Ala	122.9	7.91	4.84	1.12						
74 Val	123.2	8.73	3.97	1.69		0.46	0.61			
75 Val	127.8	8.39	4.65	1.96		0.78	0.84			

Table 1 (Continued)

residue	^{15}N	HN	Hα	Hβ	Hβ'	Hγ	Hγ'	Hδ	Hδ'	other
76 Val	120.1	8.73	4.41	2.15		0.66	0.53			
77 His	113.8	8.75	5.47	3.05	3.51					8.34 (ε1), 7.33 (δ2)
78 Asp	114.8	7.33	4.66	2.92	2.92					
79 Val	119.0	8.29	3.42	1.79		0.57	0.61			
80 Ala	123.3	8.36	4.34	1.52						
81 Ala	120.4	8.22	4.35	1.64						
82 Val	119.8	7.68	3.52	2.48		0.78	1.10			
83 Phe	117.9	7.88	4.53	3.03	3.36			7.38		7.38 (ε), 7.45 (ζ)
84 Ala	122.5	8.64	4.24	1.58						
85 Tyr	120.1	7.82	4.13	3.24	3.21			6.98		6.55 (ε)
86 Ala	122.8	8.86	3.98	1.74						
87 Lys	117.9	8.20	4.07	2.02	2.00	1.66	1.57	1.73		
88 Gln	114.5	7.25	4.09	1.84	1.84	2.42	2.34			
89 His	117.6	7.52	4.81	2.72	3.46					8.25 (ε1), 6.60 (δ2)
90 Pro										
91 Asp	116.8	8.84	4.55	2.74	2.74					
92 Gln	119.2	7.82	4.85	2.25	2.00	2.36	2.23^b			
93 Glu	122.2	8.33	4.38	2.37	2.37					
94 Leu	123.6	8.49	4.95	1.75	1.57^b	1.40		0.76	0.76	
95 Val	126.8	9.45	4.85	1.89		0.92	0.88			
96 Ile	127.9	9.69	4.53	2.58		1.45	0.82	−0.12		0.50 (γ2)
97 Ala	128.5	9.25^b	5.88	1.71						
98 Gly	103.0	5.94	2.27, 4.15							
99 Gly	108.0	7.86	4.05, 3.76							
100 Ala	124.0	8.93^b	4.03	1.50						
101 Gln	115.3	8.86	4.13	2.09						
102 Ile	121.4	7.21	3.81	1.77		1.17	1.45	0.67		0.65 (γ2)
103 Phe	117.9	7.69	4.01	2.72	2.53			5.84		7.04 (ε), 7.50 (ζ)
104 Thr	114.3	8.30	3.72	4.22			1.24			
105 Ala	122.3	7.23	4.09	1.31						
106 Phe	112.3	7.43	4.97	2.96	3.92			7.62		6.78 (ε), 6.82 (ζ)
107 Lys	120.4	7.54	4.07	2.00	2.00	1.72	1.38			
108 Asp	118.2	8.61	4.79	2.56	2.82					
109 Asp	118.2	7.97	4.93	2.67	3.11					
110 Val	117.3	7.01	3.89	1.22		0.43	0.38			
111 Asp	121.7	8.53	5.01	2.99	2.74					
112 Thr	117.4	7.67	5.56	3.92			1.41			
113 Leu	125.4	9.56	5.10	1.87	1.40	0.90		−0.96	0.29	
114 Leu	126.2	9.39	5.37	2.51^b	1.67	1.78		0.99	1.07	
115 Val	121.7	7.98	4.31	0.67		0.57	−0.02			
116 Thr	125.2	8.50	4.83	4.04		5.07	0.56			
117 Arg	127.4	9.16	4.73	1.71	1.36	1.18	1.34			
118 Leu	130.4	9.10	4.50	1.03	1.86	0.85		−0.35	−0.57	
119 Ala	120.6	8.34	4.04	1.36						
120 Gly	103.2	8.10	4.21, 3.56							
121 Ser	111.7	7.61	5.06	3.57	3.57					
122 Phe	126.6	9.70	4.75	2.88	3.38			7.52		7.19 (ε), 7.00 (ζ)
123 Glu	119.3	8.24	4.66	2.00	2.00	2.33^b	2.26			
124 Gly	108.1	8.22	4.11, 4.05							
125 Asp	115.5	8.57^b	4.98	3.05	2.62					
126 Thr	116.8	7.68	4.72	3.76			1.26			
127 Lys	128.1	8.76	5.12	1.70	1.90	1.50	1.25			
128 Met	119.5	8.89^b	4.10	1.35	1.99	1.35	1.42			−0.35 (ε)
129 Ile	117.4	7.14	4.35	1.95		0.67	1.29	0.79		1.11 (γ2)
130 Pro			4.49	1.85	2.30	2.09	2.01	3.84	3.59^b	
131 Leu	122.1	7.47	4.35	0.49	0.23	1.20		−0.03	0.43	
132 Asn	119.1	8.81	4.99	3.04	2.72					
133 Trp	123.8	7.76	3.77	2.95	3.20					10.03 (ε1), 7.40 (δ1), 5.72 (ε3), 4.52 (ζ3), 6.62 (η2), 7.60 (ζ2)
134 Asp	115.3	8.26	4.77	2.85	2.76					
135 Asp	117.6	8.00	4.78	2.75	2.52					
136 Phe	118.6	8.32	5.20	3.33	3.27			6.96		6.88 (ε)
137 Thr	115.1	9.37	4.88	3.98			1.20			
138 Lys	131.5	8.56	3.59	−0.77	1.12	0.54	0.05	1.14^b		
139 Val	126.0	9.11	4.22	2.13		0.94	0.90			
140 Ser	112.7	7.49	4.62	3.77	3.52^b					
141 Ser	115.0	8.06	5.28	3.46	3.61					
142 Arg	125.8	8.50	4.76	1.92	1.92	1.62	1.45			
143 Thr	124.3	9.03	4.74	3.80			0.87			
144 Val	130.4	9.07	3.98	0.59		0.92	0.84			
145 Glu	126.8	8.50	4.46	1.85	1.90	2.20	2.04			
146 Asp	126.4	8.17	4.86	1.99	3.11					
147 Thr	118.0	7.90	3.89	4.12			1.27			
148 Asn	122.4	9.82	5.13	2.85	3.36					
149 Pro										
150 Ala	119.2	7.69	3.95	1.38						
151 Leu	112.3	8.11	4.39	1.99	1.73	1.57		1.16	0.83	

Table 1 (Continued)

residue	^{15}N	HN	Hα	Hβ	Hβ'	Hγ	Hγ'	Hδ	Hδ'	other
152 Thr	125.0	7.43	4.29	4.20			1.11			
153 His	120.1	8.54	5.71	2.10	2.66					9.46 (ε1), 5.97 (δ2)
154 Thr	116.5	8.57	5.01	3.71			1.03			
155 Tyr	125.2	9.05	5.01	2.58	2.83			6.54		6.54 (ε)
156 Glu	124.0	9.59	5.31	2.36	2.00	2.29	2.12			
157 Val	122.9	8.04	5.27	1.99		0.94	0.94			
158 Trp	127.7	9.91	5.90	3.11	3.44					11.16 (ε1), 7.06 (δ1), 7.39 (ε3), 7.44 (ζ3), 7.18 (η2), 7.24 (ζ2)
159 Gln	120.4	9.51	5.61	2.02	2.23	2.47	2.56			
160 Lys	127.2	8.77	3.78	1.55	1.80	1.35	0.83			
161 Lys	127.1	8.53	4.14	1.82	1.61	1.22	1.40	1.68		
162 Ala	131.0	7.88	4.12	1.31						

[a] The ^1H chemical shifts (ppm) are referenced to DSS (sodium 2,2-dimethyl-2-silapentane-5-sulfonate) at 380 K. The ^{15}N chemical shifts are referenced to anhydrous NH_3 using the method described by Live *et al.* (1984). [b] These signals have ^1H chemical shifts differing by more than 0.1 ppm from the corresponding values in the *L. casei* DHFR–methotrexate complex.

Table 2: ^1H Chemical Shifts of Trimethoprim Free and Bound to *L. casei* Dihydrofolate Reductase

proton	chemical shift ppm from DSS	
	free	bound
N1H		14.85
HN2A	6.75[a]	10.46
HN2B	6.75[a]	5.90
HN4A	7.08[a]	9.18
HN4B	7.08[a]	7.18
H6	7.38[b]	6.52
H7A	3.70[b]	3.22
H7B	3.70[b]	3.74
H2',6'	6.61[b]	5.86
4'-OCH₃	3.77[b]	3.84
3',5'-OCH₃	3.83[b]	

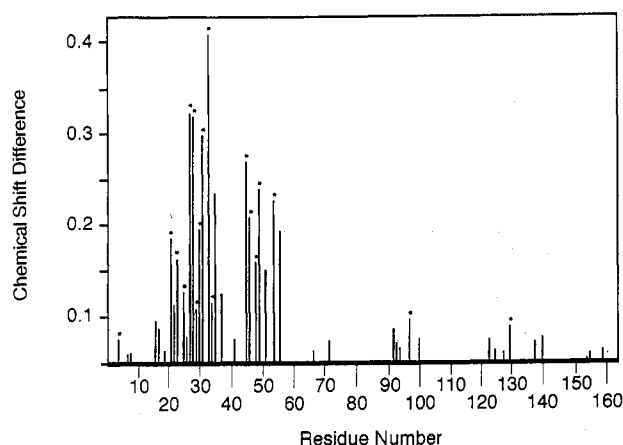[a] Measured at 283 K to sharpen signals. [b] Measured at 298 K.

FIGURE 1: Comparison of the chemical shifts of all assigned protein protons in DHFR complexes with trimethoprim and methotrexate. The shift differences for each residue are calculated as the average of the sum of the root mean square (RMS) of the shift difference for each proton in the residue. The *'s indicate those residues that are close enough to the ligand binding site that differences in ring current shielding effects due to the aromatic rings of methotrexate and trimethoprim might be expected to influence protein protons.

Intermolecular NOEs. In order to dock the ligand in its protein binding site in solution, it is necessary to measure an extensive set of intermolecular NOEs to provide the necessary distance constraints. The 2D NOESY spectra for a complex of this size (~18 kDa) are very complicated, with many overlapping cross-peaks. Such spectra do not readily lend themselves to the detection of intermolecular NOEs.

In some cases, useful NOE information can be obtained by using 1D NOE difference spectroscopy to examine the effects
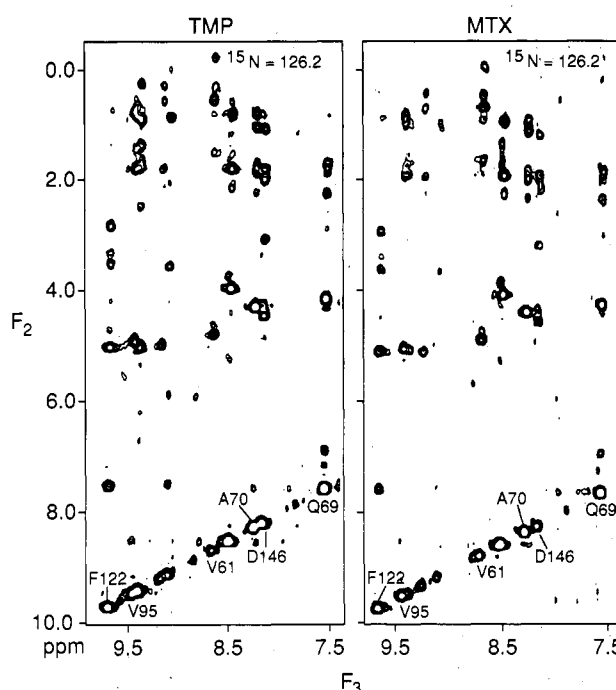

FIGURE 2: Two corresponding slices from the $^{15}N/^1H$ NOESY-HMQC spectra of the DHFR binary complexes with trimethoprim (a, left) and methotrexate (b, right). The ^{15}N chemical shift is 126.2 ppm for the F_2/F_3 slices for both complexes. The similar pattern of NOE cross-peaks can be seen for several NH protons [Q69 (7.56), D146 (8.17), A70 (8.25), V61 (8.68), V95 (9.45), F122 (9.70) ppm].

of irradiating signals with unique chemical shifts. Such a signal is provided by the N1H proton of bound trimethoprim, which occurs at very low field (14.9 ppm). The NOE difference spectrum (not shown) was obtained by subtracting the spectrum of the complex obtained with irradiation of the N1H proton (irradiation times of 0.2, 0.4, and 0.8 s were used) from that of the control spectrum. Only the intermolecular NOEs detected at all three mixing times were used for the distance constraints in Table 3.

To detect selective intermolecular NOEs it is also possible to use the isotopically labeled trimethoprim molecules 2 and 3 in conjunction with isotope editing or filtering NMR experiments. Figure 3 shows the 2D $^1H/^{13}C$ HMQC-NOESY spectrum of the complex of DHFR with [7-^{13}C,4'-*methoxy*-^{13}C]trimethoprim (3). The rows at the 4'-OCH₃ and C7 carbon frequencies show the relevant NOE connections to protons in nearby residues (see Figure 3a,b, respectively). The NOE connections for the 4'-OCH₃ protons include cross-peaks to L27δ, L19δ, and F49α,δ (Figure 3a), whereas the C7
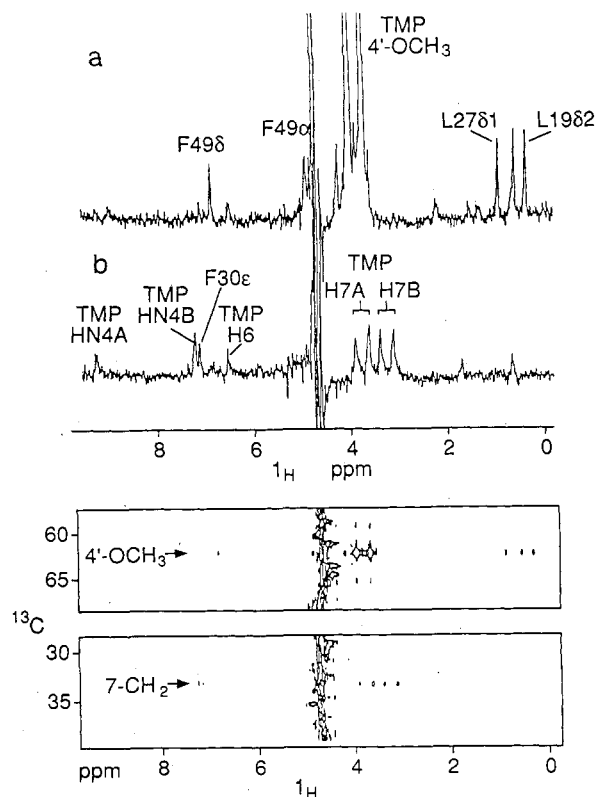
FIGURE 3: Part of the spectrum from the 2D $^1H/^{13}C$ HMQC-NOESY experiment on the binary complex of *L. casei* DHFR with [7-^{13}C,4'-*methoxy*-^{13}C]trimethoprim. The upper traces are the rows at the ^{13}C frequencies of the carbons C7 and 4'-OCH$_3$, showing the connections to their attached protons and NOEs to signals in nearby residues. The H7A and H7B signals appear as doublets because no ^{13}C decoupling in F_2 was used.
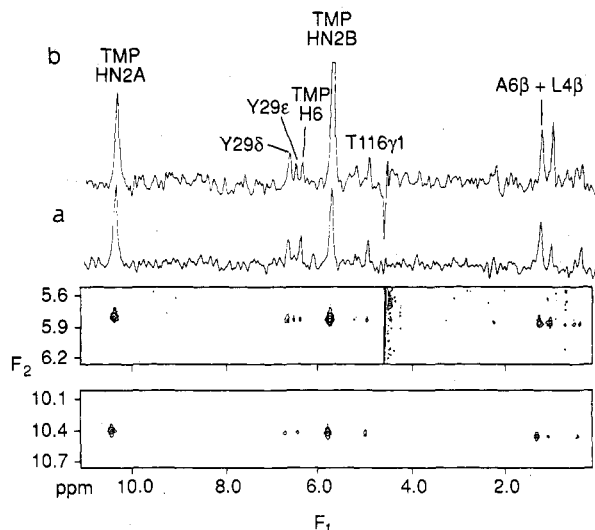

FIGURE 4: Part of the spectrum from the 2D NOESY experiment, with ^{15}N editing in ω_2 carried out on the binary complex of *L. casei* DHFR with [1,3-^{15}N$_2$,2-*amino*-^{15}N]trimethoprim. The upper traces are the rows at the frequencies of the HN2A and HN2B protons showing both intramolecular NOEs and NOEs to signals in nearby residues.

protons are seen to have NOEs to F30ε in addition to several intramolecular NOEs (Figure 3b).

Figure 4 shows the spectrum from the half-filter $^1H/^{15}N$ NOESY experiment on the complex of DHFR with [1,3-^{15}N$_2$,2-*amino*-^{15}N]trimethoprim (**2**). The two rows corresponding to the 2-NH$_2$ A and B proton frequencies are shown in Figure 4a,b, respectively; the pattern of NOEs is

Table 3: Intermolecular NOEs

	classification[a]	distance constraint (Å)
Trimethoprim–Protein		
TMP H1–L19 (Hδ$_2$[b])	s	1.8–4.2
TMP H1–A6 (Hβ[b])	s	1.8–4.2
TMP H1–Y29 (Hδ[b])	s	1.8–4.7
TMP H1–F30 (Hδ[b])	s	1.8–4.7
TMP H1–T116 (Hγ$_2$[b])	m	1.8–4.8
TMP H1–Y29 (Hε[b])	m	1.8–5.3
TMP H1–F30 (HN)	m	1.8–3.3
TMP H1–A6 (HN)	w	1.8–5.0
TMP H1–W21 (Hε$_1$)	w	1.8–5.0
TMP HN2[b]–A6 (Hβ[b])	w	1.8–7.5
TMP HN2[b]–L4 (Hβ[b])	w	1.8–7.0
TMP HN2[b]–Y29 (Hδ[b])	w	1.8–8.0
TMP HN4[b]–A97 (Hα)	w	1.8–6.0
TMP HN4[b]–W5 (Hα)	m	1.8–4.3
TMP HN4[b]–L4 (Hβ[b])	w	1.8–7.0
TMP HN4[b]–A97 (Hβ[b])	w	1.8–7.5
TMP H6–L19 (Hδ$_2$[b])	s	1.8–4.2
TMP H7[b]–F30 (Hε[b])	w	1.8–8.0
TMP 4'-OCH$_3$[b]–L27 (Hδ$_1$[b])	s	1.8–5.7
TMP 4'-OCH$_3$[b]–L19 (Hδ$_2$[b])	m	1.8–6.3
TMP 4'-OCH$_3$[b]–F49 (Hα)	s	1.8–4.2
TMP 4'-OCH$_3$[b]–F49 (Hδ[b])	m	1.8–6.8
Trimethoprim–Trimethoprim		
TMP H1–TMP H6	s	1.8–2.7
TMP H1–TMP HN2[b]	s	1.8–3.7
TMP HN4[b]–TMP H7[b]	m	1.8–5.3
TMP H6–TMP H7[b]	w	1.8–6.0

[a] s, strong; m, medium; w, weak. [b] Here, center averaging was employed between the protons, and the appropriate correction was added to the upper distance limit (Wüthrich et al., 1983).

similar in each row, reflecting transferred NOE effects due to exchange between the A and B sites.

Table 3 summarizes the intermolecular NOEs measured between the ligand and the protein using the various methods outlined earlier. The only intermolecular NOEs used in the calculations were those that also appear in 2D NOESY spectra recorded with a mixing time of 60 ms. The NOE values are classified as either strong, medium, or weak, and the appropriate distance constraints are given in Table 3. In each experiment some intramolecular NOEs were detected, and these were used to assist in classifying the intermolecular NOEs. Even when the protein signal assignments are known, there is still ambiguity in assigning NOEs if the signals have degenerate chemical shifts. The NOEs given in Table 3 involve either protein protons with unique chemical shifts or overlapped signals that could be assigned to their spin systems by their spin diffusion patterns in spectra recorded at longer mixing times. For example, in the NOE difference spectra NOEs from the N1H of trimethoprim to several protons within the F30 spin system are detected at 800 ms. This allows the assignment to be made at shorter mixing times where only the NOEs to the F30 NH and δ protons were detected.

Molecular Modeling. The conformation of trimethoprim (**1**) is defined by the torsion angles C4–C5–C7–C1' (τ_1) and C5–C7–C1'–C2' (τ_2). In the initial structure they were set to 191° and 73°, respectively, corresponding to values calculated by Birdsall et al. (1983, 1984) from consideration of ring current effects on the ^{1}H chemical shifts of the bound drug.

Because available NOE data for the trimethoxyphenyl ring is sparse, the *m*-methoxy substituents were held fixed in the plane of the benzyl ring during all of the energy minimizations (see the Materials and Methods section). The 4'-methoxy substituent was initially set at ±90° with respect to the plane of the benzyl ring, but subsequently was allowed to rotate

Table 4: Mean Energy Values for the Calculated
DHFR–Trimethoprim Structures (kcal mol^{-1})

	energy minimization	simulated annealing
bond energy[a]	27.85 ± 0.1 (2523 ± 1)[d]	8.47 ± 0.05
angle energy[a]	1582 ± 3 (4112 ± 1)[d]	1459 ± 2
improper energy[a]	6.34 ± 0.04 (7772 ± 4)[d]	1.33 ± 0.01
van der Waals[b]	–998 ± 33 (>3 × 10^6)[d]	–630 ± 26
NOE[c]	1.36 ± 0.08 (>2 × 10^4)[d]	0.70 ± 0.07
constrained dihedral[c]	0.80 ± 0.0 (0.07 ± 0)[d]	0.01 ± 0.00

[a] Calculated with X-PLOR 3.1 on the basis of values of the CHARMM force field (using paramallh3x.pro). [b] Calculated using a Lennard-Jones potential. [c] For the NOE energy, a square-well quadratic potential was used with a force constant of 100 kcal mol^{-1} Å^{-2}. An analogous potential was used for the constrained dihedral angle with a force constant of 200 kcal mol^{-1} deg^{-2}. [d] The mean of the corresponding energy term calculated for the starting structures used in the energy minimization calculations.

throughout the relaxation. The same pattern of calculated structures was obtained when the 4′-methoxy group was inverted through 180°; thus, one cannot deduce the orientation of this group. The orientations of the methoxy groups used in the calculations are those observed in the neutron diffraction studies of free trimethoprim (Koetzle & Williams, 1976).

An initial, parent structure for the complex was obtained, using Insight II, by manually inserting the ligand, in the conformation described earlier, into the enzyme structure such that the NOE data were approximately satisfied. A set of 49 starting coordinates was created by systematically rotating the dihedral angles τ_1 and τ_2 by ±40°, ±90°, and ±120° from the values in the initial parent structure. When these were subjected to the restrained energy minimization incorporating the NOE-based distance constraints given in Table 3, 23 satisfactory structures were identified that have good covalent geometries for the bound drug and NOE violations of less than 0.1 Å (see Table 4 for a summary of the mean energy values in initial and final structures). In all of these structures, the two aromatic rings of bound trimethoprim occupy essentially the same region of conformational space within the binding site and have an RMSD value of 0.89 Å (calculated for the ring atoms and C7 of trimethoprim after superposition of the protein backbone atoms). This can be seen in Figure 5a, which shows a representative set of calculated superposed structures of trimethoprim in its binding site obtained from the restrained energy minimization calculations. The overall mean values of τ_1 and τ_2 are 209 ± 50° and 43 ± 37°, respectively. The structure of the binding site in a representative complex is given in Figure 5b. Table 5 lists the neighboring residues found up to 3.5 Å from the ligand atoms by using Insight II.

The dihedral angles calculated here are in only moderate agreement with these values calculated in the earlier NMR studies of Birdsall et al. (1983, 1984) (192 ± 13° and 70 ± 13°). The latter values were based on comparing observed and calculated ring current shielding contributions. Values for τ_1 depend mainly on the ring current shielding contribution from the benzyl ring to the pyrimidine H6 proton, and this should give a fairly reliable value. The earlier values for τ_2 could have substantial errors because they involve a ring current shielding contribution to the benzyl H2′ and H6′ protons from the Phe 30 side chain, whose conformation is likely to be different in the various complexes.

For the simulated annealing calculations, in addition to the 49 starting structures used in the energy minimization calculations, 20 additional starting structures were used where the ligand was positioned outside the binding site (from 1.5
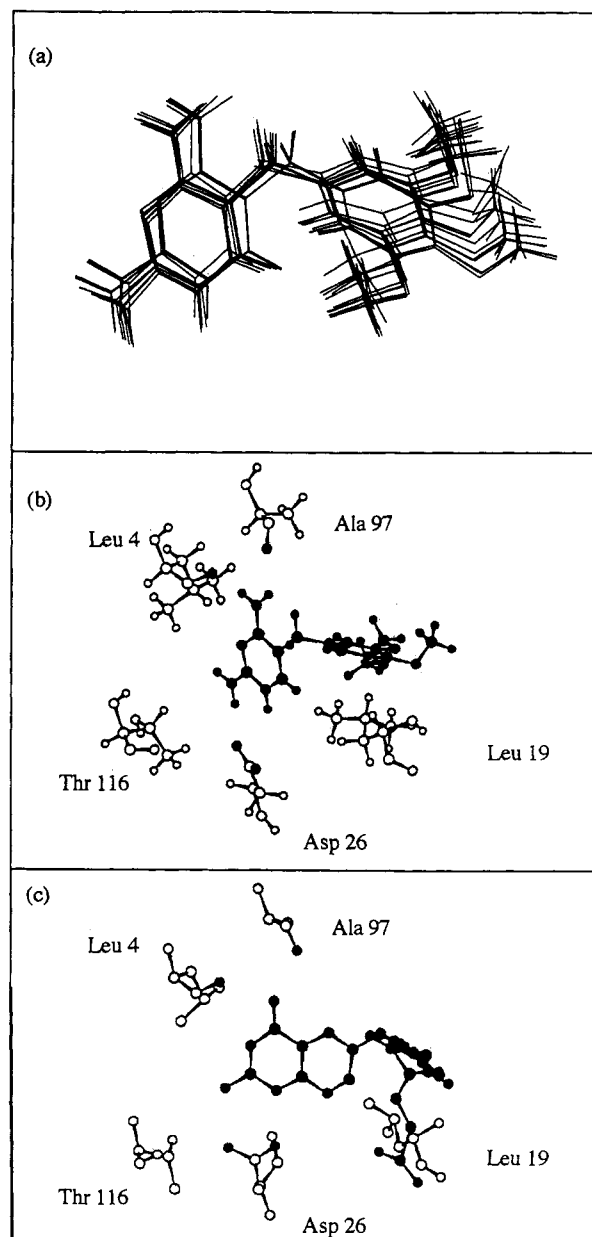

FIGURE 5: (a) Representative set of 12 restrained energy minimization calculated structures of bound trimethoprim aligned by superposition of the protein backbone atoms. (b) Representative structure from the restrained energy minimization calculations of the complex with trimethoprim (τ_1 = 224°, τ_2 = 34°). (c) Equivalent view to that shown in b of the structure of the complex with methotrexate derived from the crystal studies on the ternary DHFR–MTX–NADPH complex (Bolin et al., 1982). In this case only the heavy atom coordinates are shown. In b and c, residues 4, 19, 26, 97, and 116 in the protein are shown for reference. The ligand atoms and the carbonyl oxygens of A97 and L4 and the δ oxygens of D26 are shaded.

to 10 Å away from the final structure), with random values for their τ_1 and τ_2 angles. These calculations gave 60 satisfactory structures, with the bound trimethoprim occupying essentially the same site as in the restrained energy minimization structures. The RMSD of the trimethoprim ring atoms and C7 was 0.63 Å, calculated for all of the energy minimization and simulated annealing solutions. Although the space occupied by the trimethoprim is reasonably well defined in all of the structures by the NOE data, the values of the torsion angles cannot be accurately determined (as opposed to being precisely determined). Calculated mean values for τ_1 and τ_2 of 244 ± 10° and 20 ± 3°, respectively, were obtained from the simulated annealing calculations.

Table 5: List of Protein Residues with Atoms ≤3.5 Å from Ligand Protons

ligand atom	protein atoms	ligand atom	protein atoms
H1	A6, side chain[a]	H6	A6, side chain
	D26, side chain[a]		L19, side chain[a]
	L27, side chain[a]		L27, side chain[a]
	Y29, side chain[a]		D26, side chain
	F30, main chain[a]		F30, side chain
	F30, side chain	H7A[b]	A6, main chain
HN2A	A6, side chain		A6, side chain
	D26, side chain[a]	H7B[b]	F30, side chain
	L27, side chain		A97, side chain
	Y29, side chain[a]	H2'	L27, side chain[a]
	F30, main chain		F30, side chain[a]
	F30, side chain	H6'	L19, side chain[a]
	T116, side chain[a]	3'-OCH₃	L27, side chain[a]
HN2B	L4, side chain		F30, side chain[a]
	W5, main chain	4'-OCH₃	S48, main chain[a]
	A6, side chain[a]		F49, main chain[a]
	Y29, side chain[a]		F49, side chain
	F30, main chain	5'-OCH₃	G17, main chain[a]
	T116, side chain		H18, main chain[a]
HN4A	L4, main chain[a]		L19, side chain[a]
	L4, side chain		S48, side chain[a]
	W5, main chain[a]		
	F30, side chain[a]		
	A97, main chain[a]		
HN4B	L4, main chain[a]		
	W5, main chain[a]		
	F30, side chain[a]		
	A97, main chain		
	A97, side chain[a]		

[a] These contacts were observed in more than 75% of the energy-minimized calculated structures. [b] These assignments could be reversed.

Matthews and co-workers (1985) have reported X-ray crystal structural information on trimethoprim complexes with DHFR from *E. coli* and chicken liver and have documented the protein residues in van der Waals contact with trimethoprim in the complexes (the coordinates for the structures are not available from the Brookhaven Protein Data Bank). In the NMR-determined structures, the protein residues in van der Waals contact with the trimethoprim have been measured in order to make comparisons with the X-ray crystal data (see Table 5). These contact residues were determined by identifying ligand and protein atoms with van der Waals overlap > 10% in all of the calculated structures. The residues in contact with the pyrimidine ring were found to be D26 (side chain), L4 (backbone), W5 (backbone), L27 (side chain), and Y29 (side chain). After due account is taken for the corresponding sequence positions following sequence alignment of the bacterial and avian enzymes, it is noted that there is good agreement between corresponding contact residues in *L. casei* DHFR (solution) and the *E. coli* and chicken liver DHFR (crystal) structures. For example, all of the contact residues detected in solution are found to have corresponding contact residues in the crystal studies, with the exception of Y29 (contact with the residue corresponding to F30 is seen in the crystal studies).

Useful comparisons can also be made with the methotrexate binding site determined by X-ray crystallography in the complex of *L. casei* DHFR–MTX–NADPH, for which coordinates are available (Bolin *et al.*, 1982). The relevant part of the structure is given in Figure 5c. In the crystallographic structure of the *L. casei* DHFR–methotrexate–NADPH complex, interactions were inferred between Oδ1 of D26 in the enzyme and NA2 of the drug, as well as between Oδ2 of D26 in the protein and N1 of the ligand. Two hydrogen bonds were also inferred from NA4 of the drug to the carbonyl oxygens of L4 and A97. The analogous distances were measured in the 23 best structures of the trimethoprim–DHFR complex in solution obtained from the energy minimization calculations. The distances from D26 Oδ1 or Oδ2 to TMP N1 and 2-NH₂ had mean values of 2.9–4.3 Å, and those from TMP 4-NH₂ (HN4A) to L4 O and A97 O had mean values of 2.6–3.3 Å. These distances are approximately within the ranges that are used to infer the existence of a hydrogen bond or some other form of dipolar interaction. These results fit in with earlier NMR findings (Cocco *et al.*, 1981; Roberts *et al.*, 1981; Bevan *et al.*, 1985), which had shown that trimethoprim (like methotrexate) is protonated at N1 in its complex with DHFR and that the N1H is involved in electrostatic interactions with the protein. It can thus be concluded from these results that the binding of the 2,4-diaminopyrimidine ring of trimethoprim to DHFR in solution is similar to that observed for methotrexate in the crystal structure. This further confirms that the overall structures of the protein in the methotrexate and trimethoprim binary complexes are indeed similar.

Further refinement of the structure of the trimethoprim–DHFR complex in solution could be obtained if the intermolecular NOEs presently involving pseudoatoms on the ligand could be better defined. For example, limitations in the present data set arise from the presence of intramolecular dynamic processes, such as ring flipping of the trimethoxybenzyl ring and bond rotation in the 2- and 4-NH₂ groups on the pyrimidine ring. If conditions could be found where these processes are sufficently slow to allow specific intermolecular NOEs between individual ligand nuclei and protein nuclei to be measured, this would allow better structures to be calculated.

ACKNOWLEDGMENT

REFERENCES

Andrews, J., Clore, G. M., Davies, R. W., Gronenborn, A. M., Gronenborn, B., Kalderon, D., Papadopoulos, P. C., Schafer, S., Sims, P. F. G., & Stancombe, R. (1985) *Gene 35*, 217–222.

Baccanari, D. P., Daluge, S., & King, R. W. (1982) *Biochemistry 21*, 5068–5075.

Baker, D. J., Beddell, C. R., Champness, J. N., Goodford, P. J., Norrington, F. E. A., Roth, B., & Stammers, D. K. (1982) in *Chemistry and Biology of Pteridines* (Blair, J. D., Ed.) pp 545–549, W. de Gruyter, Berlin.

Bax, A., & Davies, R. W. (1985) *J. Magn. Reson. 65*, 355–360.

Bax, A. Griffey, R. H., & Hawkins, B. L. (1983) *J. Am. Chem. Soc. 105*, 7188–7190.

Benkovic, S. J., Fierke, C. A., & Naylor, A. M. (1988) *Science 239*, 1105–1110.

Bevan, A. W., Roberts, G. C. K., Feeney, J., & Kuyper, I. (1985) *Eur. Biophys. J. 11*, 211–218.

Birdsall, B., Roberts, G. C. K., Feeney, J., Dann, J. G., & Burgen, A. S. V. (1983) *Biochemistry 22*, 5597–5604.

Birdsall, B., Bevan, A. W., Pascual, C., Roberts, G. C. K., Feeney, J., Gronenborn, A., & Clore, G. M. (1984) *Biochemistry 23*, 4733–4742.

Birdsall, B., Arnold, J. R. P., Jimenez-Barbero, J., Frenkiel, T. A., Bauer, C. J., Tendler, J. B., Carr, M. D., Thomas, J. A., Roberts, G. C. K., & Feeney, J. (1990) *Eur. J. Biochem. 191*, 659–668.

Blakley, R. L. (1985) Dihydrofolate Reductase, in *Folates and Pterins* (Blakley, R. L., & Benkovic, S. J., Eds.) Vol. 1, Chapter 5, pp 191–253, Wiley, New York.

Bolin, J. T., Filman, D. J., Matthews, D. A., Hamlin, R. C., & Kraut, J. (1982) *J. Biol. Chem. 257*, 13650–13662.

Braunschweiler, L., & Ernst, R. R. (1983) *J. Magn. Reson. 53*, 521–528.

Brown, S. C., Weber, P. L., & Mueller, L. (1988) *J. Magn. Reson. 77*, 166–169.

Brünger, A. T. (1988) *X-PLOR Manual*, Yale University, New Haven, CT.

Brünger, A. T., & Karplus, M. (1988) *Proteins: Struct., Funct., Genet. 4*, 148–156.

Carr, M. D., Birdsall, B., Jimenez-Barbero, J., Polshakov, V. I., Bauer, C. J., Frenkiel, T. A., Roberts, G. C. K., & Feeney, J. (1991) *Biochemistry 30*, 6330–6341.

Cayley, J., Albrand, J. P., Feeney, J., Roberts, G. C. K., Piper, E. A., & Burgen, A. S. V. (1979) *Biochemistry 18*, 3886–3895.

Cocco, L., Groff, J. P., Temple, C., Jr., Montgomery, J. A., London, R. E., Matwiyoff, N. S., & Blakley, R. L. (1981) *Biochemistry 20*, 3972–3978.

Cresswell, R. M., & Methua, J. W. (1975) U.S. Patent 3878252.

Dann, J. G., Ostler, G., Bjur, R. A., King, R. W., Scudder, P., Turner, P. C., Roberts, G. C. K., & Burgen, A. S. V. (1976) *Biochem. J. 157*, 559–571.

Davies, D. G., & Bax, A. (1985) *J. Am. Chem. Soc. 107*, 2820–2821.

Falzone, C. J., Cavanaugh, J., Cowart, M., Palmer, A. G., III, Matthews, C. R., Benkovic, S. J., & Wright, P. E. (1994) *J. Biomol. NMR 4*, 349–366.

Feeney, J. (1990) *Biochem. Pharmacol. 40*, 141–152

Filman, D. J., Bolin, J. T., Matthews, D. A., & Kraut, J. (1982) *J. Biol. Chem. 257* (22), 13663–13672.

Freisheim, J. H., & Matthews, D. A. (1984) in *Folate Antagonists Therapeutic Agents* (Sirotnak, F. M., Ed.) Vol. 1, pp 69–131, Academic, Orlando, FL.

Frenkiel, T., Bauer, C., Carr, M. D., Birdsall, B., & Feeney, J. (1990) *J. Magn. Reson. 90*, 420–425.

Gronenborn, A. M., Bax, A., Wingfield, P. T., & Clore, G. M. (1989a) *FEBS Lett. 243*, 93–98.

Gronenborn, A. M., Wingfield, P. T., & Clore, G. M. (1989b) *Biochemistry 28*, 5081–5089.

Groom, C. R., Thillet, J., North, A. C., Pictet, R., & Geddes, A. J. (1991) *J. Biol. Chem. 266*, 19890–19893.

Jeener, J., Meier, B. H., Bachmann, P., & Ernst, R. R. (1979) *J. Chem. Phys. 71*, 4546–4553.

Koetzle, T. F., & Williams, G. J. B. (1976) *J. Am. Chem. Soc. 98*, 2074–2077.

Live, D. H., Davis, D. G., Agosta, W. C., & Cowburn, D. (1984) *J. Am. Chem. Soc. 106*, 1939–1941.

Macura, S., Huong, Y., Suter, D., & Ernst, R. R. (1981) *J. Magn. Reson. 43*, 259–281.

Marion, D., & Wüthrich, K. (1983) *Biochem. Biophys. Res. Commun. 113*, 967–974.

Marion, D., Driscoll, P. C., Kay, L. E., Wingfield, P. T., Bax, A., Gronenborn, A. M., & Clore, G. M. (1989a) *Biochemistry 28*, 6150–6156.

Marion, D., Kay, L. E., Sparks, S. W., Torchia, D. A., & Bax, A. (1989b) *J. Am. Chem. Soc. 111*, 1515–1517.

Matthews, D. A., Bolin, J. T., Burridge, J. M., Filman, D. J., Volz, K. W., Kaufman, B. T., Beddell, C. R., Champness, J. N., Stammers, D. K., & Kraut, J. (1985) *J. Biol. Chem. 260*, 381–399.

Mayer, R. J., Chen, J. T., Taira, K., Fierke, C. A., & Benkovic, S. J. (1986) *Proc. Natl. Acad. Sci. U.S.A. 83*, 7718–7720.

Morris, G. A., & Freeman, R. (1978) *J. Magn. Reson. 29*, 433–462.

Mueller, L. (1979) *J. Am. Chem. Soc. 101*, 4481–4484.

Nilges, M. (1992) *X-PLOR 3.1 Manual*, pp 316–319, Yale University, New Haven, CT.

Oefner, C., D'Arcy, A., & Winkler, F. K. (1988) *Eur. J. Biochem. 174*, 377–388.

Press, W. H., Flannery, B. P., Teukolsky, S. A., & Vetterling, W. T. (Eds.) (1988) in *Numerical Recipes in C: The Art of Scientific Computing*, pp 447–466, University Press, U.K.

Rance, M., Sorensen, O. W., Bodenhausen, G., Wagner, G., Ernst, R. R., & Wüthrich, K. (1983) *Biochem. Biophys. Res. Commun. 117*, 479–485.

Roberts, G. C. K., Feeney, J., Burgen, A. S. V., & Daluge, S. (1981) *FEBS Lett. 131*, 85–88.

Roth, B., & Cheng, C. C. (1982) *Prog. Med. Chem. 19*, 1–58.

Rykaert, J. P., Ciccotti, G., & Berendsen, H. J. C. (1977) *J. Comp. Phys. 23*, 327–341.

Shaka, A. J., Barker, P. B., & Freeman, R. (1985) *J. Magn. Reson. 64*, 547–552.

Smal, M., Cheung, H. T. A., & Davies, P. E. (1986) *J. Chem. Soc., Perkins Trans. 1*, 747–751.

Soteriou, A., Carr, M. D., Frenkiel, T. A., McCormick, J. E., Bauer, C. J., Sali, D., Birdsall, B., & Feeney, J. (1993) *J. Biomol. NMR 3*, 535–546.

States, D. J., Haberkorn, R. A., & Ruben, D. J., (1982) *J. Magn. Reson. 48*, 286–292.

Stockman, B. J., Nirmala, N. R., Wagner, G., Delcamp, T. J., De Yarman, M. T., & Freisheim, J. H. (1992) *Biochemistry 31*, 218–229.

van Gunsteren, W. F., & Berendsen, M. J. C. (1977) *Mol. Phys. 34*, 1311–1327.

Villafranca, J. E., Howell, E. E., Voet, D. H., Strobel, M. S., Ogden, R. C., Abelson, J. N., & Kraut, J. (1983) *Science 222*, 782–788.

Wagner, G., & Wüthrich K. (1979) *J. Magn. Reson. 33*, 675–680.

Weber, D. J., Gittis, A. G., Mullen, G. P., Abeygunawardana, C., Lattman, E., & Mildvan, A. S. (1992) *Proteins: Struct., Funct., Genet. 13*, 275–287.

Wider, G., Weber, C., Traber, R., Widmer, H., & Wüthrich, K. (1990) *J. Am. Chem. Soc. 112*, 9015–9016.

Wüthrich, K. (1986) *NMR of Proteins and Nucleic Acids*, Wiley, New York.

Wüthrich, K., Billeter, M., & Braun, W. (1983) *J. Mol. Biol. 169*, 949–961.